Deep-level transient-spectroscopy study of rhodium in indium phosphide

A. Dadgar, D. Ammerlahn, A. Näser, R. Heitz, M. Kuttler, and D. Bimberg
Institut für Festkörperphysik, Technische Universität Berlin, Hardenbergstraβe 36, 10623 Berlin, Germany

N. Baber*
Semiconductor Physics Laboratory, Department of Physics, Quaid-i-Azam University, Islamabad, Pakistan

J. Y. Hyeon and H. Schumann
Institut für Anorganische und Analytische Chemie, Technische Universität Berlin, Strasse des 17. Juni 115, 10623 Berlin, Germany
(Received 30 June 1995)

The electrical properties of rhodium-related defects in low-pressure metal-organic chemical-vapor-deposition-grown InP:Rh are investigated. Rh concentrations up to 1×10^{19} cm^{-3} are achieved without formation of macroscopic Rh_xP_y precipitates. With deep-level transient spectroscopy, two Rh-related deep levels, Rh*A* and Rh*B*, are observed in p-InP:Rh having zero- and low-field activation energies of $E_V+0.71$ and $E_V+0.62$ eV, respectively. Optimization of the growth parameters allows for both traps to obtain electrically active concentrations up to 2×10^{15} cm^{-3}. Detailed capacitance transient investigations were undertaken to study the field dependence of the emission rates and the hole capture cross sections of both levels. The emission rate is found to be strongly field dependent for both levels. For Rh*A* the experimental data are well fitted with a Poole-Frenkel model employing a three-dimensional square well potential of 7.5 nm. The field-enhanced emission of Rh*B* can be explained by a Coulomb potential in combination with a phonon-assisted tunneling process. Evidence is given that Rh*A* is the $Rh^{3+/2+}$ deep acceptor level in InP caused by isolated substitutional Rh on In sites. Both traps are suited as compensating acceptors for the growth of semi-insulating InP.

I. INTRODUCTION

$3d$ transition metals (TM's) in InP have been studied very intensively in the last decade.[1] Only little is known about the properties of the heavier $4d$ and $5d$ transition metals.[2,3] Bremond *et al.*[3] investigated several $4d$ transition metals (Nb, Mo, Ru, Rh, Pd) in InP grown by the liquid encapsulated Czochralski technique and the gradient freeze method. They observed precipitates at doping levels above 3×10^{16} cm^{-3} and detected several traps by deep-level optical spectroscopy in n-type InP. None of these traps, however, could be clearly identified as transition metal induced. The main problem of growing transition-metal-doped InP from the liquid phase are the low solubility, the small distribution coefficient, and the large reactivity of phosphorous in the melt with many transition metals being most probably responsible for the formation of precipitates. Using low-pressure metal-organic chemical-vapor deposition (MOCVD) growth formation of precipitates of the transition metal with phosphorous can be strongly reduced.

Theoretical predictions for the energy positions of heavy transition-metal-induced deep levels have been made by Makiuchi *et al.*[4] They propose that $4d$ and $5d$ transition metals in III-V semiconductors induce energy states above those of the isovalent $3d$ elements. Recently, this prediction has been found valid to explain the shift of the energy positions for the isovalent series of transition metals Ti, Zr, and Hf in MOCVD-grown InP.[2]

Doping with the $3d$ transition metal Fe is presently the only way to obtain semi-insulating InP.[5–8] The n-type background of nominally undoped InP can be compensated by Fe, which introduces a midgap acceptor level.[5] Fe has shown an undesired low thermal stability and in contact with p-type layers a strong interdiffusion with shallow acceptors[9,10] is observed limiting device applications. A solution to this problem could be $4d$ or $5d$ transition metals introducing deep acceptor states. These elements have larger ionic radii than their isovalent $3d$ counterparts and therefore a lower diffusivity can be expected. By measuring ion implanted as well as MOCVD grown samples with secondary ion mass spectroscopy the diffusion coefficient of several $4d$ and $5d$ transition metals has been determined by us.[11,12] The Rh diffusion coefficient, for example, is three orders of magnitude lower than for Fe [1×10^{-14} cm^2/s as compared to 1×10^{-11} cm^2/s (Ref. 12)]. The low diffusivity of $4d$ and $5d$ transition metals thus makes them interesting candidates as dopants to produce semi-insulating and at the same time thermally stable III-V compounds.[13] The aim of this work is to study in detail the electrical properties of Rh-induced deep levels in MOCVD-grown InP by means of deep-level transient spectroscopy (DLTS) in particular as a function of the electric field. Rh is the $4d$ transition metal isovalent to Co, which induces a deep acceptor level $Co^{3+/2+}$ 0.32 eV above the valence band in InP.[14] Thus Rh is a likely candidate for a midgap acceptor in InP. Preliminary investigations by us indeed have indicated that Rh induces a deep midgap level above the $Co^{3+/2+}$ acceptor in MOCVD grown p-InP:Rh (Refs. 13 and 15) and in liquid phase epitaxial (LPE) grown $In_{0.53}Ga_{0.47}As$:Rh.[16]

0163-1829/96/53(11)/7190(7)/$10.00 © 1996 The American Physical Society

II. MOCVD GROWTH AND EXPERIMENTAL PROCEDURE

The precondition for doping is the existence of a metal-organic precursor of the dopant that is stable in a H_2 atmosphere and provides a sufficiently high vapor pressure. Especially for Rh this is very difficult to realize because of the strong catalytic behavior of Rh in a hydrogen atmosphere, which is used by us as carrier gas. Fast degradation of most organic Rh compounds limits the variety of substances suitable for standard MOCVD. We found two stable Rh compounds, namely Rh(cp)(cod) (cyclopentadienyl-cyclooctadienyl-rhodium) and CYNOR [cyclopentadienyl-norbonadien-rhodium(l)]. Both are solid sources. CYNOR has a higher vapor pressure allowing higher Rh concentrations in the reactor. Our samples are grown with an Aixtron LP-MOCVD at a reactor pressure of 20 mbar and a growth temperature of 640 °C. The InP growth rate is about 2.5 μm/h using TMIn and PH_3 as source materials.

For the DLTS measurements we fabricate p^+/n or n^+/p type diodes, which are Rh doped in the n-or p-type layer, respectively except for reference samples. Dopant sources are SiH_4 for the n-doped layers and dimethylzinc (DMZn) or dimethylcadmium (DMCd) for the p-doped layers. Rh doping levels up to 3×10^{18} and 1×10^{19} cm^{-3} are achieved for Rh(cp)(cod) and CYNOR, respectively.

Double-x-ray-diffraction (DXD) measurements show a slight broadening of the InP(004) reflection only at a Rh doping level of 1×10^{19} cm^{-3}. The full width at half maximum (FWHM) rises here from 13 to 19 arcsec comparing undoped and Rh-doped InP samples. At lower doping levels no broadening is found. Additionally no macroscopic defects are observed with a Normarski microscope.

For DLTS measurements mesa diodes with diameters of 200–800 μm are fabricated by photolithography and wet chemical etching. Ohmic contacts are evaporated on the front and backside of the diodes.

DLTS measurements are carried out with a computer controlled system using a Boonton 7200 capacitance bridge and a HP 8115A pulse generator. Complete capacitance transients are recorded and stored for analysis. The stored data can be used for the synthesis of conventional DLTS spectra by subtracting capacitance values at two different delay times t_1 and t_2 and plotting this difference ΔC as a function of temperature. The result is equivalent to the double boxcar integrator method.

III. RESULTS

A. Identification of *A* and *B* traps

Figure 1 shows the DLTS spectra of Rh-doped and undoped p-InP. In p-type InP layers deep Rh-induced levels are observed. For short filling pulses a peak labeled Rh*A* can be observed. With increasing filling pulse length the Rh*A* peak broadens at its low temperature side (Fig. 1). This broadening is due to two different effects: First by capture in the free-carrier Debye tail, occurring in a region with a higher field, combined with field enhanced emission. The second cause is an additional level named Rh*B*. This level Rh*B* has a much lower capture cross section than Rh*A* and therefore occurs only for longer filling pulse lengths.

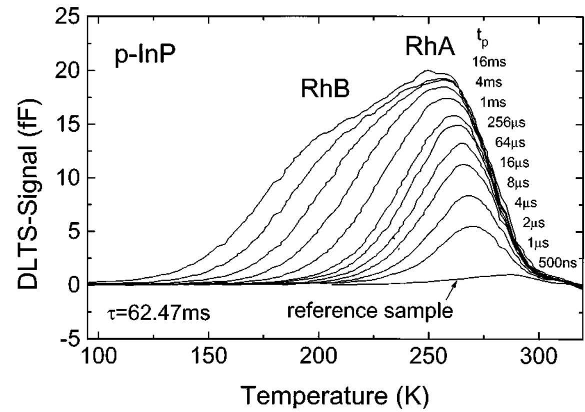

FIG. 1. DLTS spectra of Rh-doped p-InP for different filling pulse lengths. Carrier concentration of the sample is $N_A=3\times10^{16}$ cm^{-3}.

To study the trap Rh*B* it is necessary to separate the two overlapping peaks Rh*A* and Rh*B*. Such a separation is not possible with conventional boxcar techniques, even if a small difference of the Boxcar time window is used. To get direct access to the properties of Rh*B* we subtract the Rh*A* peak. This can be done in a straightforward way because Rh*A* has a much larger capture cross section than Rh*B*. As can be seen in Fig. 1 for short filling pulses Rh*A* completely dominates the spectrum. For long filling pulses the Rh*B* peak appears at the low-temperature side of Rh*A*. DLTS spectra showing only the Rh*B* emission are generated from transients that are obtained by the subtraction of transients where Rh*A* just saturates from transients recorded with much longer filling pulses where both peaks are present (Fig. 2).

The concentration of Rh*A* and Rh*B* as determined by DLTS measurements is found to be much lower than the absolute Rh content of the layers (Fig. 3). To get a high electrical activation of Rh we varied our MOCVD growth parameters and fabricated a variety of samples at different Rh precursor flows, temperatures, III-V ratios and reactor pressures. We found that the only way to significantly increase the concentration of the two Rh-related deep levels is to increase the absolute Rh concentration of the layers. For a Rh concentration of 1×10^{17} cm^3 the concentration of the

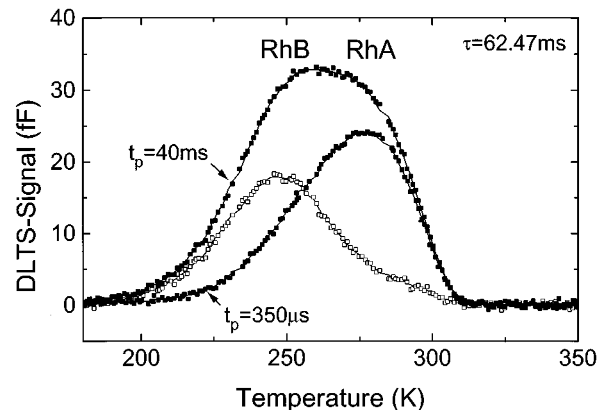

FIG. 2. DLTS spectra for a short and for a long filling pulse showing Rh*A* and both levels Rh*A* and Rh*B*. The subtracted spectra resulting out of these data shows Rh*B* only. Carrier concentration of the sample is $N_A=4\times10^{15}$ cm^{-3}.

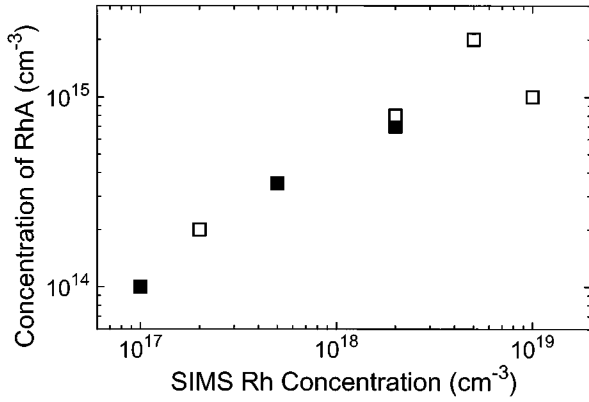

FIG. 3. Concentration of the level Rh*A* in p-InP at different Rh concentrations as measured with secondary-ion-mass spectroscopy. Full squares: samples grown with Rh(cp)(cod), open squares: samples grown with CYNOR.

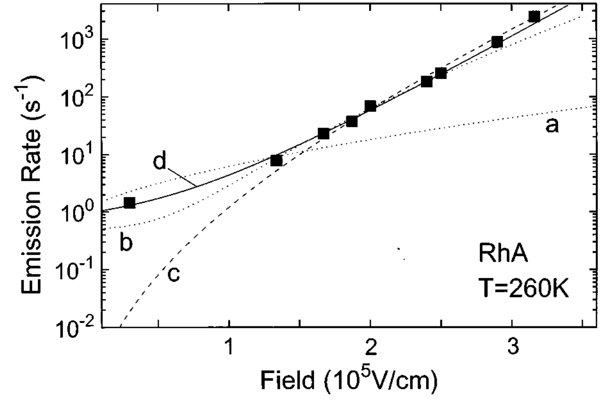

FIG. 5. Experimentally observed emission rates (squares) and fit with a Coulomb potential with $q=e$ (a), $q=2e$ (b), a Coulomb potential with $q=2e$ combined with a phonon-assisted tunneling process (c) and for a square-well potential of 7.5 nm (d).

level Rh*A* is determined to be approximately 1×10^{14} cm^3 increasing more than one order of magnitude to 2×10^{15} cm^3 at a Rh doping level of 5×10^{18} cm^3 (Fig. 3). A clear upper limit for the concentration of Rh*A* could not be observed. At a Rh content above 1×10^{19} cm^{-3} the crystallographic quality of InP starts to deteriorate causing additional DLTS peaks making an exact determination of the concentration of Rh*A* impossible. In all samples studied the concentration of Rh*B* is found to be about 80% of the concentration of Rh*A*.

B. Field effect

The emission characteristics of Rh*A* are investigated using short filling pulses. Figure 4 shows the Rh*A* signature for different electrical fields in the space charge region of the diodes obtained by double correlation deep-level transient spectroscopy measurements (DDLTS).[17] Transients recorded for different filling pulse heights are subtracted here from each other resulting in transients of carrier emission in a small portion of the space charge region with well-defined

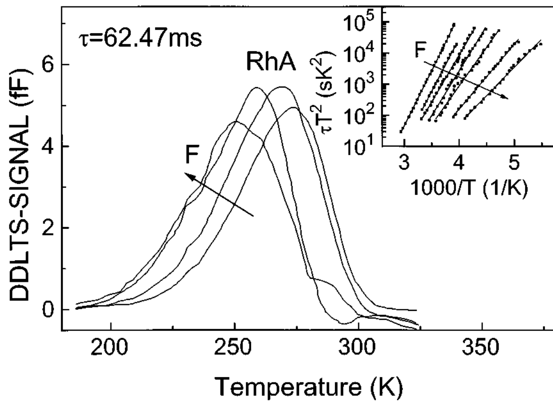

FIG. 4. DDLTS spectra of p-InP:Rh at different field strength (τ=62.47 ms). The inset shows Arrhenius plots of Rh*A* as generated by DDLTS measurements. Activation energies and field strengths are (from the left to the right): E_A=0.71 eV, $F=3\times10^4$ V/cm; E_A=0.67 eV, $F=1.9\times10^5$ V/cm; E_A=0.59 eV, $F=1.7\times10^5$ V/cm; E_A=0.57 eV, $F=2\times10^5$ V/cm; E_A=0.49 eV, $F=2.4\times10^5$ V/cm; E_A=0.40 eV, $F=2.9\times10^5$ V/cm; E_A=0.35 eV, $F=3.2\times10^5$ V/cm.

electrical field. The Arrhenius plots generated from these DDLTS data show a strong dependence of the emission rate on the strength of the electric field (insert Fig. 4). The activation energies range from $E_V+(0.71\pm0.01)$ eV for a field strength of 3×10^4 V/cm to $E_V+(0.35\pm0.02)$ eV at 3.2×10^5 V/cm, corresponding to an increase of the hole emission rate by over a factor of 1000 if the electric field is raised by a factor of 10. This field enhanced emission can be explained by a Poole-Frenkel effect.[18] The energy barrier for carrier emission given by the defect potential of the charged center is lowered. For a variety of possible defect potentials the Poole-Frenkel barrier lowering has been modeled in the work of Martin, Streetman, and Hess:[18] The simplest potential form that can be assumed for a charged center is a Coulomb potential. If a strong phonon coupling of the deep center exists this can be taken into account by an additional term. This term considers phonon-assisted tunneling and mainly results in a reduction of the emission rate at lower field strengths as compared to a Coulomb potential only. A screening of the charge by surrounding electrons is considered for by a Yukawa potential. Such a screened Coulomb potential leads to a weaker field dependence of the emission rate than a simple Coulomb potential. Another possible potential form for a charged transition-metal center is a square-well potential successfully employed to fit the field enhanced emission of the deep $Ti^{3+/4+}$ donor in InP.[19]

For a simple Coulomb potential the emission rate at field F is given by

$$\frac{e_p(F)}{e_p(0)}=\frac{1}{\gamma^2}\left[e^{\gamma}(\gamma-1)+1\right]+\frac{1}{2}$$

$$\text{with}\quad \gamma=\left(\frac{qF}{\pi\varepsilon_r\varepsilon_0}\right)^{1/2}q/kT, \tag{1}$$

where q is the electronic charge, ε_0 the permittivity of free space, ε_r the relative permittivity of the host crystal, k the Boltzmann constant, T the temperature, and F the electric field. Lines a and b in Fig. 5 correspond to fits assuming a single and a double charged center, respectively. $q=2$ gives a reasonable fit of the high-field data but underestimates the emission rate at lower fields. As mentioned above, a screened Coulomb potential[18] results in an even lower rise of the

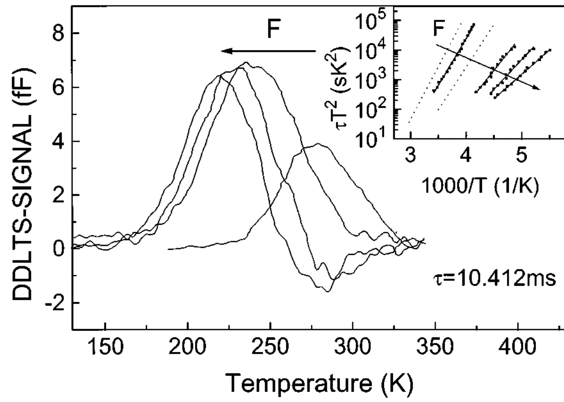

FIG. 6. DDLTS spectra of Rh*B* for different field strengths. The inset shows the Arrhenius plots as generated by DDLTS measurements. Activation energies and field strengths for Rh*B* are (straight lines from the left to the right): E_A=0.62 eV, $F=4\times10^4$ V/cm; E_A=0.45 eV, $F=1.4\times10^5$ V/cm; E_A=0.39 eV, $F=1.7\times10^5$ V/cm; E_A=0.32 eV, $F=2\times10^5$ V/cm. For reference the low-field and a high-field ($F=2\times10^5$ V/cm) Arrhenius plots of Rh*A* are also plotted (dotted lines).

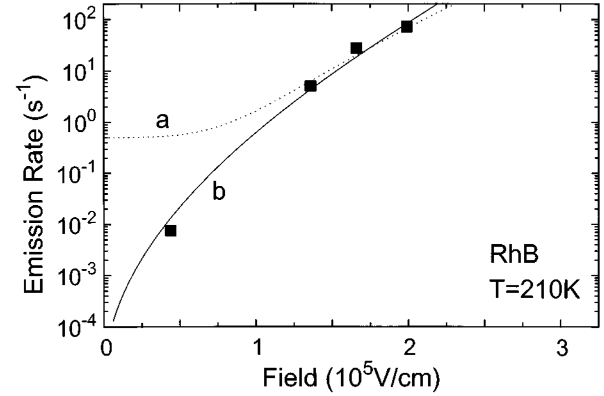

FIG. 7. Emission rates of Rh*B* (squares) and fits for $q=2e$ with a Coulombic potential (a) and with an additional phonon assisted tunneling process (b).

emission rate with increasing electric field strength and therefore seems not to be suited to fit the emission characteristic of Rh*A*.

Vincent, Chantre, and Bois describe a one-dimensional Coulomb potential combined with a one-dimensional phonon-assisted tunneling process.[20] As in the case without phonon-assisted processes, a good fit can be achieved for higher field strengths by assuming a double charged center (line *c* in Fig. 5). However, our low-field data again cannot be fitted with such a potential. Therefore a Coulomb potential even in combination with a phonon-assisted tunneling process is not suited to fit our data. Baber *et al.*[19] successfully employed a three-dimensional square-well potential[18] to fit the field effect data obtained for the deep $Ti^{3+/4+}$ donor level in InP

$$\frac{e_p(F)}{e_p(0)}=\frac{1}{2\gamma}(e^{\gamma}-1)+\frac{1}{2}, \tag{2}$$

leading to a field-dependent emission rate with $\gamma=qFr/kT$, r being the radius of the well. Assuming a single charged center we can obtain a good fit of our data with Eq. (2) using a square-well potential radius of 7.5 nm. From fit, the zero-field position of the Rh*A* trap can be determined to 0.71 $\pm$0.01 eV above the valence band.

Rh*B* shows a strong field influence as well (Fig. 6), being even stronger than in the case of the Rh*A* trap. The variation of the activation energy between $E_V+(0.62\pm0.02)$ eV and $E_V+(0.32\pm0.02)$ eV for field strength range from 4.4×10^4 to 2.0×10^5 V/cm, respectively (inset of Fig. 6). This corresponds to a rise in the emission rate by more than 600 when the field is raised by only a factor of 4.5. To investigate the emission characteristics of Rh*B* we had to extrapolate the data of the low-field Arrhenius plot to lower temperatures due to the large shift of the emission rate with increasing electric field.

The very strong rise of the emission rate of Rh*B* with increasing field cannot be described by a Coulomb or square-well potential. Only assuming a doubly charged Coulomb potential combined with a phonon-assisted tunneling process gives a reasonable fit of the data (Fig. 7). From this fit it is found that the unoccupied Rh*B* trap belongs to a charged center as Rh*A*. For Rh*B*, however, an additional strong-phonon coupling has to be taken into account. Our data of Rh*B* are very limited, making it difficult to determine the zero-field activation energy. It should be slightly larger than the low-field activation energy of $E_V+0.62$ eV. Thus Rh*B* is found to be also a midgap trap in InP.

C. Hole capture

In DLTS measurements the value of the carrier capture cross section σ_∞ is usually determined from the intersection of the Arrhenius plot at $1/T=0$. This value for σ_∞ usually differs much from the experimentally observed value of σ at lower temperatures. In addition the emission rate is also a function of temperature. A correction of the apparent activation energy is necessary if such a temperature-dependent capture cross section is observed. Knowing the electron and hole capture cross sections of a deep level, it is possible to determine whether a deep level behaves as a carrier trap or a recombination center.

The hole capture cross section of Rh*B* can be determined directly by using the DLTS data shown in Fig. 8. These

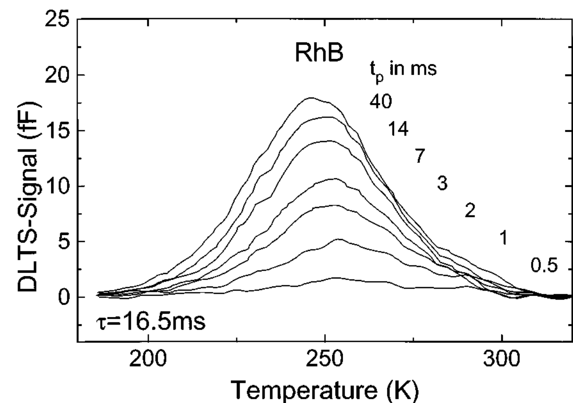

FIG. 8. DLTS spectra of Rh*B* for increasing filling pulse lengths after subtraction of transients obtained by a shorter filling pulse where Rh*A* is just saturated.

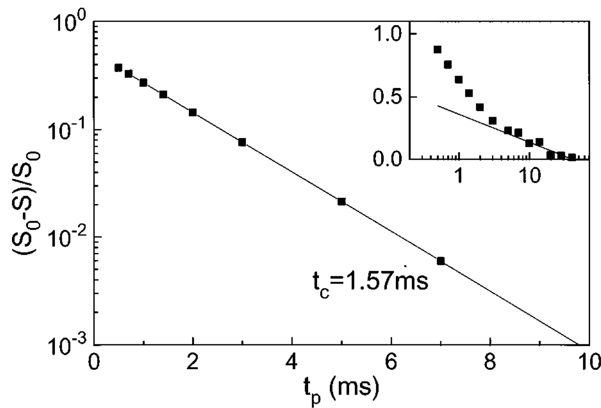

FIG. 9. Capture data for RhB at 281 K. The inset shows the plot for the Debye-tail correction (straight line).

DLTS data are generated from transients for filling pulses of different lengths from which transients for a shorter pulse where RhA is saturated were subtracted. The data show an exponential capture behavior for RhB, taking into account a Debye-tail correction as described in the work of Baber *et al.*[21] (Fig. 9). It is found that the hole capture cross section of RhB is temperature independent in the range from 250 to 281 K and yields $\sigma_h=(1.0\pm1.0)\times10^{-20}$ cm^2.

Looking at the hole capture of RhA, this process seems to be nonexponential (squares in Fig. 10). Carrier capture in the free-carrier Debye tail[21] is thought to cause this dependence. Using a Debye-tail correction for long filling pulses (inset of Fig. 10) it is, however, not possible to fully correct the capture data (circles in Fig. 10). Thus the capture cannot be described by a single level. As mentioned before, the second DLTS peak RhB, which has an approximately two orders of magnitude lower capture cross section than RhA appears for long filling pulses at the low temperature side of the RhA peak. Taking this into account, the Debye-tail correction for long filling pulses is a correction mainly of the RhB Debye tail because the influence of the RhA Debye tail for very long pulses is negligibly small. Therefore the resulting data

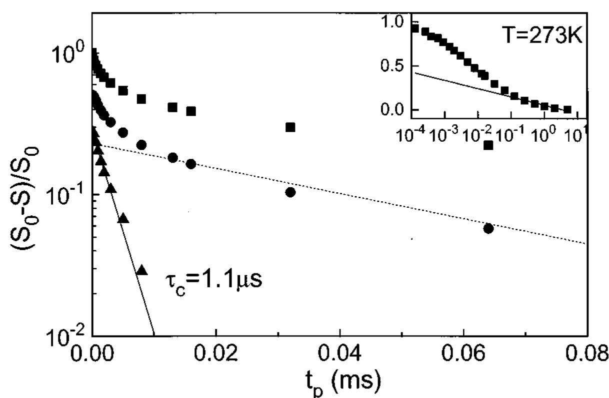

FIG. 10. Capture data of RhA as obtained by spectra as in Fig. 1 (squares). The inset shows the Debye-tail correction of the data corresponding to a correction of the influence of the RhB Debye tail resulting in the data given as circles. Subtracting the remaining influence of the level RhB and the RhA Debye tail given by the dotted line results in the capture data of RhA (triangles). Carrier concentration of the sample is $N_A=4\times10^{15}$ cm^{-3}.

(circles in Fig. 10) still contain exponential parts caused by RhA and RhB and from the RhA Debye tail. The influence of the hole capture of RhB and the Debye tail of RhA is represented by the dashed line in the corrected data of Fig. 10. Subtracting these data the exponential capture data for RhA remain (triangles in Fig. 10). The hole capture cross section of RhA is found to be $\sigma_h=(1.7\pm1.5)\times10^{-18}$ cm^2 independent of temperature in the range from 255 to 312 K. The large error is caused by the various corrections we made. Thus the emission rate is also not influenced by temperature and the activation energy of these levels does not have to be corrected.

Both Rh-induced deep levels RhA and RhB are only observed in hole emission and only in p-type InP. It is not possible to determine the electron capture cross sections of RhA or RhB. Since electron emission is not observed, both centers act as hole traps instead of recombination centers.

IV. DISCUSSION

Two Rh-induced deep levels RhA and RhB are observed in InP. The electrically active concentration of these deep levels increases nearly linearly with the absolute Rh content of the layers. In DXD measurements, an increase of the FWHM of the InP(004) reflex is observed for Rh doping levels larger than 1×10^{19} cm^{-3}. At such doping levels the crystal structure starts to get significantly deteriorated. This deterioration is possibly due to the strong reactivity of Rh with phosphorous, which leads to the formation of Rh_xP_y precipitates. Due to such reactions, electrically active Rh concentration might be strongly reduced already at lower total concentrations. In DLTS measurements, the deterioration of the crystalline quality results in additional DLTS peaks. These peaks make an exact determination of the Rh-related deep-level concentration at Rh doping levels above 1×10^{19} cm^{-3} impossible.

RhA and RhB show a strong field effect that can be used to identify these traps. For RhA the fit with a square-well potential suggests that RhA is due to an acceptor like transition as $Rh^{2+/3+}$ or $Rh^{1+/2+}$. To clearly identify RhA, we compare our data with two theoretical predictions. First of all, the energy position of a 4d transition metal is expected to be above that of its isovalent 3d element.[4] The isovalent 3d transition metal to Rh is Co. The $Co^{2+/3+}$ acceptor in InP is situated at $E_V+0.32$ eV well below the Rh levels.[14] The $Co^{1+/2+}$ transition, which is expected to be positioned above the $Co^{2+/3+}$ acceptor, is not observed in InP. Therefore RhA with $E_A=E_V+(0.71\pm0.01)$ eV cannot be the $Rh^{1+/2+}$ transition. Taking into account the prediction of Makiuchi *et al.*[4] and our field effect data RhA is possibly the $Rh^{2+/3+}$ deep acceptor in InP (Fig. 11).

Secondly, we compare the energy position of the Rh-induced deep levels RhA in InP and Rh1 in $In_{0.53}Ga_{0.47}As$, which is observed by DLTS in electron emission in both LPE grown[16] and MOCVD grown $In_{0.53}Ga_{0.47}As$:Rh. Based on the high electrical active concentration of Rh1 in MOCVD grown $In_{0.53}Ga_{0.47}As$, a precise determination of the activation energy could be made as $E_C-(0.41\pm0.03)$ eV at 300 K. From the internal reference rule[22] it is expected that the energy position of a transition-metal-induced defect (here Rh on cation site) is independent of the host compound and at a fixed energy as compared to an internal energy level. The

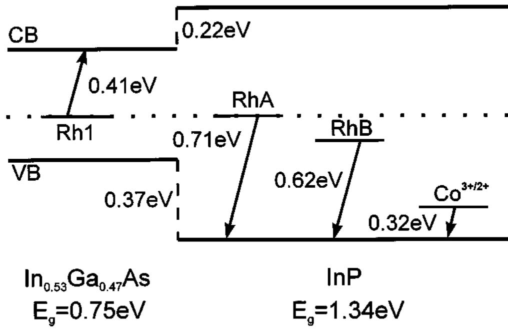

FIG. 11. Band diagram of $In_{0.53}Ga_{0.47}As$ and InP with the Rh-related levels observed in both materials and the Co acceptor level in InP (Ref. 14).

validity of the internal reference rule has been proven for $3d$ transition metals in III-V and II-VI compounds.[22] For the Rh-correlated levels Rh1 in $In_{0.53}Ga_{0.47}As$ and RhA in InP the internal reference rule[22] is perfectly fulfilled (Fig. 11). Thus, RhA and Rh1 are attributed to the $Rh^{3+/2+}$ acceptor levels in InP and $In_{0.53}Ga_{0.47}As$, respectively.

For the second level, RhB, the fit of the field effect data with a combination of a Coulomb potential with a phonon-assisted tunneling process suggests that this level is also due to an acceptorlike transition. The observed strong interaction with the lattice suggests that RhB is possibly a doubly charged acceptorlike Rh-related complex.

The fit of the field dependence of the thermal hole emission of RhA yields a radius of a square-well potential of 7.5 nm. From this value the hole capture cross section σ can be calculated[19] to be 1.8×10^{-12} cm^2. This value for σ is in good agreement with σ_∞ obtained from the intersection of the Arrhenius plot at $1/T=0$ (Table I). For the capture of a hole by a charged center, corresponding to the transition of Rh^{2+} to Rh^{3+}, a large capture cross section can be expected similar to that for electron capture of the $Ti^{3+/4+}$ deep donor in InP.[19,23] However, at temperatures around 300 K a hole capture cross section as low as 1.7×10^{-18} cm^2 has been determined for the $Rh^{2+/3+}$ deep-level RhA. Not observing any electron emission signal in n-type InP the electron capture cross section of the midgap level RhA must be well below this value of 1.7×10^{-18} cm^2. We compared the values of the capture cross sections to those of $3d$ transition-metal-induced midgap traps in InP ($Fe^{3+/2+}$, $Ti^{3+/4+}$) at similar temperatures (Table I). For Fe the values for the electron and hole capture cross sections at 300 K are 2×10^{-17} and 4×10^{-18} cm^2, respectively.[24] For Ti a larger difference in the capture cross sections is observed. The electron and hole capture cross sections are determined to be 6.6×10^{-13} cm^2 (Refs. 19 and 23) and 2.7×10^{-22} cm^2 (Ref. 23) at 300 K. In the case of Fe, a capture barrier causes a lowering of the capture cross sections by several orders of magnitude compared to the values of σ_∞.[24] In the case of Ti, only a capture barrier for hole capture is known.[23] Possibly, the low value in the hole capture cross section of RhA comparable to the hole capture cross section of Fe is due to a barrier for carrier capture. For RhA such a barrier was not observed in capture measurements at temperatures around 300 K. This might be due to a shift of the onset of the rise of the capture cross section to higher temperatures caused by a relatively high capture barrier. The level RhB is found to be possibly a double charged center situated closer to the valence band than RhA. Therefore a larger capture cross section than for RhA can be expected. Instead we observe unexpectedly a hole capture cross section for RhB, which has a four order of magnitude lower value. This low value might be due to the

TABLE I. Electrical characteristics of the Rh-related deep levels in InP. Additionally listed are the properties of the $Fe^{2+/3+}$ (Refs. 24, 25), $Ti^{3+/4+}$ (Refs. 19, 23), and $Co^{2+/3+}$ (Ref. 14) deep levels in InP. The activation energy of the $Fe^{2+/3+}$ transition at 300 K is calculated from the value given in Ref. 25 at 1.7 K.

Level	Activation Energy (eV)	Poole-Frenkel effect best fit with	σ_∞ (cm^2)	$\sigma(T)$ (cm^2)
RhA	$E_V+0.71\pm0.01$	Square-well potential of 7.5 nm	Arrhenius plot: $\sigma_{p_\infty}=1.3\times10^{-12}$ From the square-well potential size: $\sigma_{p_\infty}=1.8\times10^{-12}$	$\sigma_p=1.7\pm1\times10^{-18}$ (255–312 K)
RhB	$\geqslant E_V+0.62$ $E_V+0.62\pm0.02$ at $F=4.4\times10^4$ V/cm	Coulomb potential combined with phonon-assisted tunneling	Arrhenius plot: $\sigma_{p_\infty}=7.6\times10^{-14}$	$\sigma_p=1.0\pm1\times10^{-20}$ (250–281 K)
$Fe^{2+/3+}$	$E_V+0.74$		$\sigma_{p_\infty}=2.5\times10^{-15}$ $\sigma_{n_\infty}=6.5\times10^{-16}$	$\sigma_p=4\times10^{-18}$ (300 K) $E_B=166$ meV $\sigma_n=2\times10^{-17}$ (300 K) $E_B=89$ meV
$Ti^{3+/4+}$	$E_C-0.59\pm0.02$	Square-well potential of 4.6 nm	From the square-well potential size: $\sigma_{n_\infty}=6.6\times10^{-13}$	$\sigma_p=(2.8–27)\times10^{-23}$ (100–300 K) $E_B=30$ meV $\sigma_n\approx6\times10^{-13}$ (300 K)
$Co^{2+/3+}$	$E_V+0.32$ eV			

influence of the strong coupling of RhB to the lattice causing a high capture barrier.

V. SUMMARY

We successfully doped InP with the $4d$ transition metal Rh by LP-MOCVD growth. In p-InP:Rh two Rh-related deep acceptor levels RhA and RhB have been observed by DLTS (Table I). Both levels show a strong field effect with activation energies of $E_A = E_V + (0.71 \pm 0.01)$ eV at zero field for RhA and $E_A = E_V + (0.62 \pm 0.02)$ eV at $F = 4.4 \times 10^4$ V/cm for RhB. The field-enhanced emission data of RhA can be explained by a Poole-Frenkel effect employing a three-dimensional square-well potential of 7.5 nm. In the case of RhB the field-enhanced emission is due to a Coulomb potential in combination with a phonon-assisted tunneling process.

For RhA and RhB the capture cross sections are determined to $\sigma_h = 1.7 \times 10^{-18}$ cm^2 and $\sigma_h = 1.0 \times 10^{-20}$ cm^2 at 300 K, respectively. We attribute the level RhA to the $Rh^{3+/2+}$ acceptor level caused by isolated substitutional Rh on In sites. This level satisfies the internal reference rule[22] if compared to a Rh-related level (Rh1) observed in $In_{0.53}Ga_{0.47}As$. Analysis of the field-effect data of RhB suggests that this level is due to a Rh-correlated doubly charged acceptorlike complex. Introducing two midgap acceptor levels, with total electrically active concentration around 4×10^{15} cm^{-3}, Rh is an interesting candidate for fabricating thermally stable semiinsulating InP.

ACKNOWLEDGMENTS

We are very grateful to K. Schatke for supporting the LP-MOCVD growth work and DXD measurements. Parts of this work were funded by the Deutsche Forschungsgemeinschaft (Bi284/10) and German Telekom.

---

*Deceased.

[1] B. Clerjaud, J. Phys. C **18**, 3615 (1985).

[2] H. Scheffler, N. Baber, A. Dadgar, D. Bimberg, J. Winterfeld, and H. Schumann, Phys. Rev. B **51**, 4142 (1995).

[3] G. Bremond, A. Nouailhat, G. Guillot, Y. Toudic, B. Lambert, M. Gauneau, R. Coquille, and B. Deveaud, Semicond. Sci. Technol. **2**, 772 (1987).

[4] N. Makiuchi, T. C. Macedo, M. J. Caldas, and A. Fazzio, Defect Diffusion Forum **62/63**, 145 (1989).

[5] S. Yamakoshi, in *Semi-Insulating III-V Materials, Malmö 1988*, edited by G. Grossmann and L. Ledebo (Hilger, Bristol, 1988), p. 213.

[6] G. W. Iseler and B. S. Ahern, Appl. Phys. Lett. **48**, 1656 (1986).

[7] M. J. Harlow, W. J. Duncan, I. F. Lealman, and P. C. Spurdens, J. Cryst. Growth **140**, 19 (1994).

[8] R. P. Leon, M. Kaminska, Kin Man Yu, and E. R. Weber, Phys. Rev. B **46**, 12 460 (1992).

[9] E. W. A. Young and G. M. Fontijn, Appl. Phys. Lett. **56**, 146 (1990).

[10] T. Wolf, T. Zinke, A. Krost, H. Scheffler, H. Ulrich, D. Bimberg, and P. Harde, J. Appl. Phys. **75**, 3870 (1994).

[11] A. Knecht, M. Kuttler, H. Scheffler, T. Wolf, D. Bimberg, and H. Kräutle, Nucl. Instrum. Methods Phys. Res., Sect. B **80/81**, 683 (1993).

[12] A. Näser, A. Dadgar, M. Kuttler, R. Heitz, J. Y. Hyeon, S. Wernick, D. Bimberg, and H. Schumann, Appl. Phys. Lett. **67**, 479 (1995).

[13] D. Bimberg, A. Dadgar, R. Heitz, A. Knecht, A. Krost, M. Kuttler, H. Scheffler, A. Näser, B. Srocka, T. Wolf, T. Zinke, J. Y. Hyeon, S. Wernik, and H. Schumann, J. Cryst. Growth **145**, 455 (1994).

[14] M. S. Skolnick, R. G. Humphreys, P. R. Tapster, B. Cockayne, and W. R. Mac Ewan, J. Phys. C **16**, 7003 (1983).

[15] H. Scheffler, B. Srocka, A. Dadgar, M. Kuttler, A. Knecht, R. Heitz, D. Bimberg, J. Y. Hyeon, and H. Schumann, in *Physics and Applications of Defects in Advanced Semiconductors*, edited by M. O. Manasreh *et al.*, MRS Symposia Proceedings No. 325 (Materials Research Society, Pittsburgh, 1994), p. 329.

[16] B. Srocka, H. Scheffler, and D. Bimberg, Appl. Phys. Lett. **64**, 2679 (1994).

[17] H. Lefevre and M. Schulz, Appl. Phys. **12**, 45 (1977).

[18] P. A. Martin, B. G. Streetman, and K. Hess, J. Appl. Phys. **52**, 7409 (1981).

[19] N. Baber, H. Scheffler, A. Ostmann, T. Wolf, and D. Bimberg, Phys. Rev. B **45**, 4043 (1992).

[20] G. Vincent, A. Chantre, and D. Bois, J. Appl. Phys. **50**, 5484 (1979).

[21] N. Baber, H. G. Grimmeis, M. Klevermann, P. Omling, and M. Zafar Iqbal, J. Appl. Phys. **62**, 2853 (1987).

[22] J. M. Langer, C. Delerue, M. Lanoo, and H. Heinrich, Phys. Rev. B **38**, 7728 (1988).

[23] H. Scheffler, N. Baber, A. Dadgar, T. Wolf, and D. Bimberg (unpublished).

[24] A. Dadgar, R. Engelhardt, and D. Bimberg (unpublished).

[25] A. Juhl, A. Hoffmann, D. Bimberg, and H. J. Schulz, Appl. Phys. Lett. **50**, 1292 (1987).